



Effects of Pillar-Based Substrate on the Wire Arc Additive Manufacturing Process

Anas Ullah Khan¹ · Yuvraj K. Madhukar¹

Received: 1 October 2020 / Revised: 5 April 2021 / Accepted: 19 April 2021 / Published online: 10 May 2021
© Korean Society for Precision Engineering 2021

Abstract

The Wire arc additive manufacturing (WAAM) process uses a metal plate as a substrate for part deposition. The presented work uses small pillars of cuboidal shapes arranged together to form the required deposition surface instead of a single large substrate. The post-processing of WAAM is arduous due to the need for the part removal from the substrate. The pillar-based substrate made this part removal process simpler and reduced the machining requirement. A WAAM setup was designed and developed in-house by integrating the gas metal arc welding (GMAW) with a three-dimensional gantry. The setup was utilised to deposit thin-walled metal parts over the pillar-based substrate. The online recorded temperature at the base using thermocouples confirmed adequate cooling between subsequent layers. The temperature of the pillar-based substrate was compared with the conventional substrate, which ensured proper heat dissipation. The microstructural study and hardness measurement of the deposited parts also confirmed that the pillar-based substrate has little effect on the part quality. The applications of the pillar-based substrate were further extended to demonstrate the deposition of multiple parts on a single substrate and part containing non-planar layers (overhanging features).

Keywords Wire arc additive manufacturing · Pillar-based substrate · Part removal · Overhanging features

1 Introduction

Additive manufacturing (AM) has evolved from a process previously used only for making prototypes to now being able to fabricate industrial application parts directly from a CAD model. For metal AM, commonly used feed material is in the form of powder and wire. The standard processes utilising the metal powders are selective laser sintering (SLS), selective laser melting (SLM), laser engineered net shaping (LENS), and electron beam melting (EBM) [1–5]. The most preferred processes for metal wire additive manufacturing are the wire + arc additive manufacturing (WAAM) and wire + laser/electron beam additive manufacturing (WLAM or LHW) [6–8]. The use of wire as a raw material has many advantages such as ease of handling, higher catchment efficiency, cost-effectiveness and its manufacturing. The material deposition rate is also high in case of the wire-based process hence less time consuming to build large parts [9–11].

A WAAM system typically uses a wire feeder, a deposition torch, a programmable control unit and a welding power source, e.g. gas metal arc welding (GMAW) [12–14], gas tungsten arc welding (GTAW) [15–17] and plasma arc welding (PAW) [18].

The additive manufacturing processes require a substrate for part deposition. The WAAM process uses a metal substrate as it has to be electrically conductive. In general, this substrate does not serve as an integrated part of the product manufactured additively and needs to be separated [19]. The conventional approach is to separate the deposited part by cutting it from the bottom. Though this approach is widely accepted, it also leads to loss of deposited material from the bottom of the part. The relative percentage loss would become significant if the part is shorter in height. It also requires the deposition of a few extra layers at the base to compensate for the loss. However, the tool reachability remains a matter of concern for large parts and would require a specific jig or fixture. Arad Azizi et al. [20] used graphite plate instead of metal as the substrate to deposit stainless steel (SS) 316L parts by selective laser melting (SLM) process. After deposition, it was separated by heating at 400 °C. The graphite could also be brittle fractured to remove the deposited part. Hildreth et al. [21] used

✉ Yuvraj K. Madhukar
yuvrajmadhukar@iiti.ac.in

¹ Department of Mechanical Engineering, Indian Institute of Technology Indore, Indore 453552, India

sacrificial metal supports in case of directed energy deposition AM. They deposited the overhanging features of stainless steel over the sacrificial carbon steel which was later removed by electrochemical etching. For WAAM, Haselhuhn et al. [22] suggested that to modify the deposition parameters for the first layer to facilitate the part removal. It was achieved by reducing the input power and not supplying any shielding gas to ensure minimum penetration into the substrate. In another report, they applied thin coatings of different material combinations (i.e. Aluminum oxide and Boron nitride) to weaken the adhesion of the deposited parts [23]. The proposed approach showed good potential to be adopted; however, these solutions could not be universal as the coatings are specific to the material properties.

The overhanging features in AM require support structures that are built along with the part. It provides a deposition surface for overhanging features and minimises the stresses. The metal-based AM processes such as SLM, LENS, EBM and direct metal laser sintering (DMLS), the support structures are often required depending on the part geometry. The typical structures are lattice support, honeycomb support, unit cell supports, etc. [24]. Achieving these structures would be difficult in case of WAAM due to relatively bigger melt pool which leads to large bead features. Kapil et al. [25] minimised the need for the support structure by tilting the substrate with the help of five-axis deposition to fabricate undercuts. Panagiotis et al. [26] used positional welding by tilting the cold metal transfer (CMT) deposition torch at various angles and were able to fabricate straight wall with an angle ranging from 0° to 90° with respect to the substrate plate.

The primary objective of the substrate is to provide a base for the first layer as further layers would be deposited upon it. The presented experimental study investigates the pillar-based substrates to deposit metal parts and replace the conventional substrates to ease the part removal process and reduce machining requirement. These pillars are simple vertical column similar to the pillars utilised for the construction of bridges. However, they were arranged in a two-dimensional array to achieve large deposition surface. The pillar-based substrate was further modified to address overhanging features in the object by varying pillar height. The conducted experiment showed the inherent potential of the process to fabricate complex geometries, facilitate part removal and minimise material wastage.

2 Experimentation

2.1 Material and Experimental setup

An additive manufacturing setup employing GMAW as a heat source was used to investigate the effect of the pillar-based substrate (Fig. 1). A three-axis gantry with automated

control stage was designed and developed in-house. The deposition head was mounted on the Z-axis, and the workpiece was mounted on a fixture which provided XY movements. The motion was controlled by Mach3 CNC controller (CNC board and provided software). The AM system consisted of GMAW power source (Kemppi FastMig Pulse 450) and a wire feeder (Kemppi FastMig MXF 65). ER70S-6 steel wire of 0.8 mm diameter was used as the wire electrode (deposition material). The chemical composition is shown in Table 1. Argon was used as a shielding gas at a flow rate of 10 l/min. AISI 1020 low carbon steel was used as substrate and pillar material.

2.2 Substrate Design

Two different approaches were adopted to design the pillar-based substrate. The aim was to minimise the surface area but sufficient to accommodate the first layer (Fig. 2). The straight wall was deposited first to study the effectiveness of the approach. Figure 2a and b show the first design approach consisting of 3 mm sheet as the substrate and pillars of the same thickness. Post-deposition these thin pillars could be removed easily and better tool reachability could be achieved for part separation. However, in this case the deposition of three-dimensional parts such as cylinder, rectangular pipe etc. may not be effective. Therefore in the second approach, cuboidal pillars were arranged in an array to form the desired surface. The top cross-section of these pillars was serving as the deposition surface (Fig. 2c). Six different arrangement

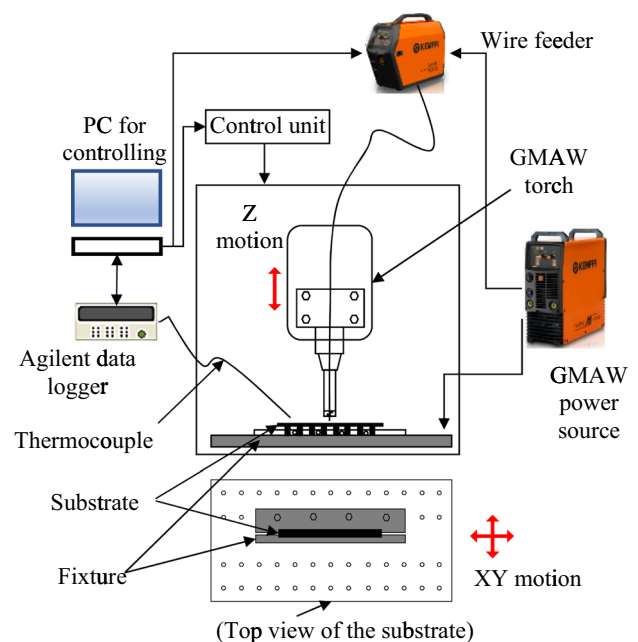


Fig. 1 Schematic of the WAAM setup

Table 1 Chemical composition of low alloy steel (ER70S-6)

Elements	C	Mn	S	Si	P	Cu	Cr	Ni	Mb	V
Composition, wt %	0.09	1.6	0.007	0.9	0.007	0.2	0.05	0.05	0.05	0.05

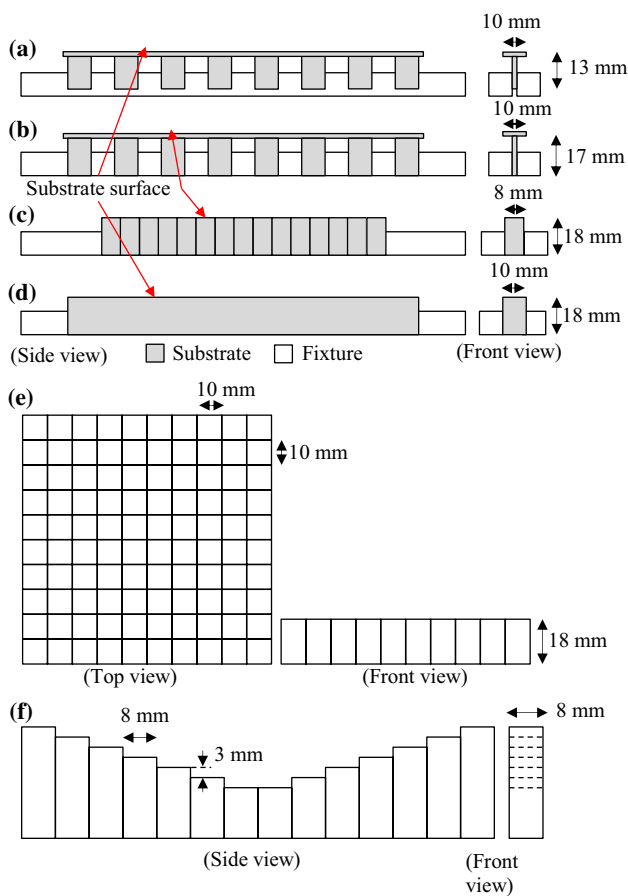


Fig. 2 **a** Substrate-1: Pillar-based substrate with pillar height of 10 mm, **b** Substrate-2: Pillar-based substrate with pillar height of 17 mm, **c** Substrate-3: Pillar-based substrate, with pillars forming the deposition surface, **d** Substrate-4: Solid substrate of height 18 mm, **e** Substrate-5: Pillar-based substrate arranged in a 2-D matrix of 10×10 pillars, **f** Substrate-6: Pillar-based substrate of varying height to support overhanging features

of substrates were used in the presented work as described in Table 2.

2.3 Experimental Procedures

A single bead wall was deposited layer over layer on the substrates 1–4 to examine the effects of the pillar-based substrates. The deposition parameters such as wire feed speed (wfs), deposition speed and input voltage were optimised and utilised for all the depositions. The temperature at the substrate was monitored throughout the deposition using thermocouples. After each layer deposition, the substrate was allowed to cool to a temperature of ~40 °C. A hollow

cylinder and hollow square shapes were deposited on substrate-5. A ‘V’ shape structure was deposited on the substrate-6 to utilise the varying height of the pillars to support overhanging features. The utilised deposition parameters for all different substrates (substrate 1–6) and the typical pattern of the bead are presented in Table 3.

3 Result and Discussions

It was observed that the multiple layers could be deposited in all the four chosen substrates. The wall dimensions also remained consistent (height ~15 mm, width ~4 mm) for a constant 9 layer of deposition. The pillar-based substrate was not imparting any difference in the appearance of the deposited part. However, possible variations in mechanical properties among the part deposited on the different substrates are analysed and discussed in succeeding sections. It was based on the change in microstructure, hardness and heat dissipation through the substrate. A marginal bending was observed in the pillar-based substrate specifically at the start and end of the deposited wall for substrate-1 and substrate-2 due to weld distortions. However, such distortion was not observed in the case of the pillar-based substrate (i.e., substrate-3). Figure 3 shows the cross-sectional view of the deposited walls for pillar-based and solid substrate (substrate 3 and 4). The surface roughness of the deposited wall was also measured using the cross-section images. The average surface roughness, R_a was found to be 0.34, 0.21, 0.13 and 0.15 mm for the walls deposited on substrate 1–4, respectively. These surface roughness lies in similar ranges as found in literature for WAAM process [27].

3.1 Bead Geometry Optimisation

The deposition parameters responsible for sound bead, i.e. input voltage, wire feed rate, and deposition speed, were optimised by analysing the bead geometry. It was ensured that the chosen parameters would produce a bead free from defects, e.g. micro-cracks, blowholes, and inclusion of spatter. AISI 1020 sheet of 3 mm thickness was used as the substrate. The other parameters, such as gas flow rate and stand-off distance (SOD), were kept constant at 10 l/min and 4 mm, respectively. The deposition travel speed was kept constant at 0.3 m/min as increasing the speed further caused a discontinuous bead. Beads were deposited for three different wire feed rates, i.e. 3.0, 3.5 and 4.0 m/min at voltage varying from 16–23 V.

Table 2 Description for the substrate design

Substrate	Description
1	It was made of a 150 mm long and 10 mm wide mild steel sheet of 3 mm thickness. The sheet was attached with rectangular pillars (by resistance spot welding) of the same metal sheet having dimensions of 13 mm × 10 mm × 3 mm, as shown in Fig. 2a. This substrate assembly was mounted on a holding fixture for the deposition. The side surface of the pillars was in contact with fixture up to the depth of 9 mm, providing the path for heat dissipation
2	It was similar to substrate-1, with a longer pillar length of 17 mm. Due to its length, the bottom surface of the pillars also came in contact with the base plate (Fig. 2b). In this way, all three surfaces of the pillar were in contact with the fixture and base. Therefore, the conductive heat transfer was expected to increase as the contact surface area increased
3	This substrate design consisted of cuboidal pillars of height 18 mm and cross-Sect. 8 mm × 8 mm fixed side by side to form the deposition surface, as shown in Fig. 2c
4	The conventional solid substrate was also used to have a comparative study by observing any possible variations in properties of the deposited part that might have caused due to the above pillar-based substrates. The dimensions of the conventional substrate were kept similar to pillar-based substrates, i.e., 18 mm height, 150 mm length and 10 mm width (Fig. 2d)
5	Cuboidal pillars were arranged in a square array of 10 × 10 pillars to deposit three-dimensional parts. Each pillar had a height of 18 mm and the top surface area of 10 × 10 mm ² , which made the total surface area available for deposition equal to 100 × 100 mm ² (Fig. 2e)
6	The pillars of varying height having the same cross-section area was used to demonstrate deposition of a part with overhanging features (non-planar layers, Fig. 2f). V-shape was chosen for the purpose

Table 3 Weld parameters for various depositions

Substrate	V	Wfs	N	Remarks	Average current (A)	Energy (kJ/mm)
Substrate-1	17	3.5	9	Wall deposition	59–59.5	0.16–0.162
Substrate-2						
Substrate-3						
Substrate-4						
Substrate-5	21	3.5	25	Cylinder part	66.2–68.2	0.22–0.229
Substrate-5			30	Square part		
Substrate-6			15	V-shape		

Deposition speed = 0.3 m/min, Stand-off distance = 4 mm, Shielding gas flow rate = 10 l/min, *V = Voltage, wfs = wire feed speed (m/min), N. = number of layers

It was observed that the deposition voltage has a direct effect on bead geometry. Bead width was found to increase with the increase in voltage, while bead height remained in a similar range (Fig. 4). At higher voltage, the produced heat would be higher, which melts more amount of material, resulting in a bigger melt pool size. Figure 4 shows that the bead width and height for 3.0 m/min wire feed rate was less than at 4.0 m/min. It indicates that increasing the wire feed rate increases the bead width and height, as more material input would increase the cross-section area of the deposited wall. The bead dimensions were chosen as small as possible to increase the dimensional accuracy of deposited objects. The wire feed rate of 3.5 m/min at a voltage of 17 V was selected for the presented work. Also, less heat input in the case of 17 V was beneficial to prevent the substrate from thermal distortion or bending.

3.2 Online Temperature Monitoring at the Base

The online temperature monitoring was conducted to examine the heat dissipation efficiency of pillar-based substrate utilised for the WAAM process. It was measured using a K-type thermocouple. A data logger (model: Agilent 34972a) with multiplexer (model: Agilent 34901a) was used for acquiring the temperature data. Both the heating and cooling cycles were measured at a distance of ~ 5 mm below the deposition surface for the substrate-1 to substrate-4, for the straight wall deposition. The temperature was recorded at three different locations, i.e. at the beginning (~ 5 mm from the onset of deposition), mid and at the end (~ 5 mm before the endpoint) of the deposited wall. Figure 5 shows the recorded temperature variations, where each peak represents the deposition of a layer.

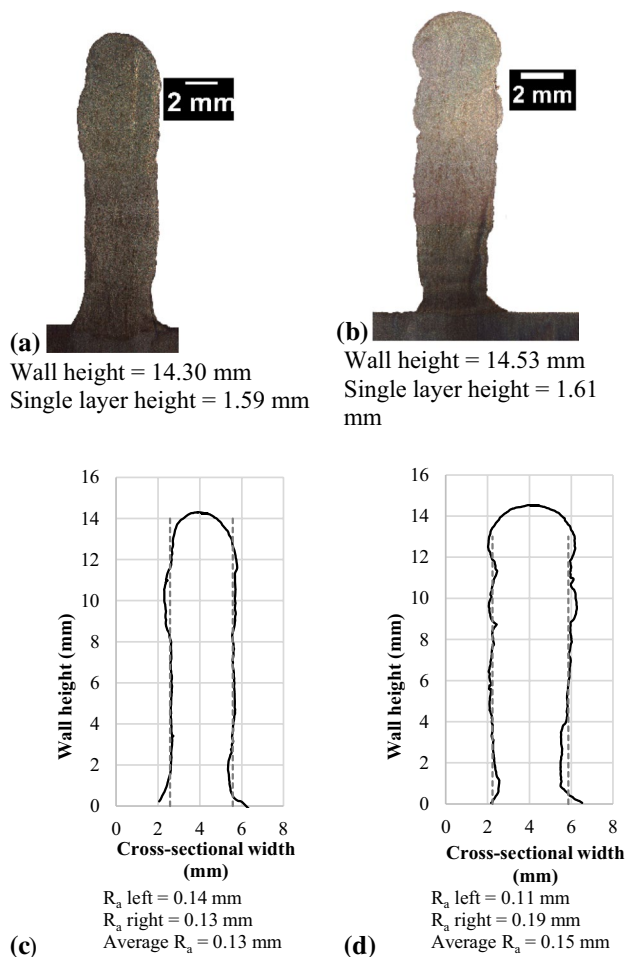


Fig. 3 The cross-sections of the single bead wall deposited on **a** pillar based and **b** solid substrate surface profile for **c** pillar-based and **d** solid substrate

It was observed that the temperature rose quickly to its peak and then cooled down slowly for each layer of the deposition. The peak temperature was observed decreasing with each subsequent layer. It could be due to an increase in distance between the deposition surface and measurement point at the base, hence the heat dissipation by conduction reduces and the convection + radiation heat dissipation increases [28]. The similar trend of temperature variation was observed for all four types of substrates. It was noted that the recorded peak temperatures were relatively higher in the case of the pillar-based substrate as compared to the conventional solid substrate (substrate-4). A similar trend was observed for all three different locations of the temperature measurement (Fig. 5). The possible reason could be the availability of a large mass in the case of the conventional substrate, which allows the heat to dissipate relatively faster. The substrate-1 was found to be most inefficient in heat dissipation as it took the maximum time to cool. The bottom surface of the pillars was not in contact with the base fixture,

possibly resulting in reduced heat dissipation. In the substrate-2 and substrate-3, the pillars were in contact with the base fixture allowing the heat to dissipate relatively faster. It was also evident from the shifting of the cooling curve towards the left in all three measurement locations. The conducted experiment shows that the pillar-based substrate could be considered equally effective in heat dissipation as compared to the conventional solid substrate.

3.3 Microstructural Study

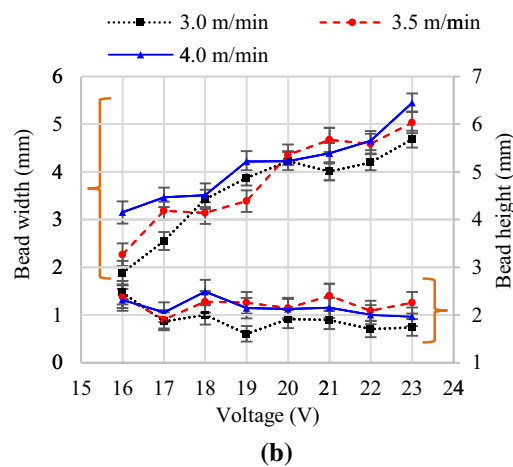
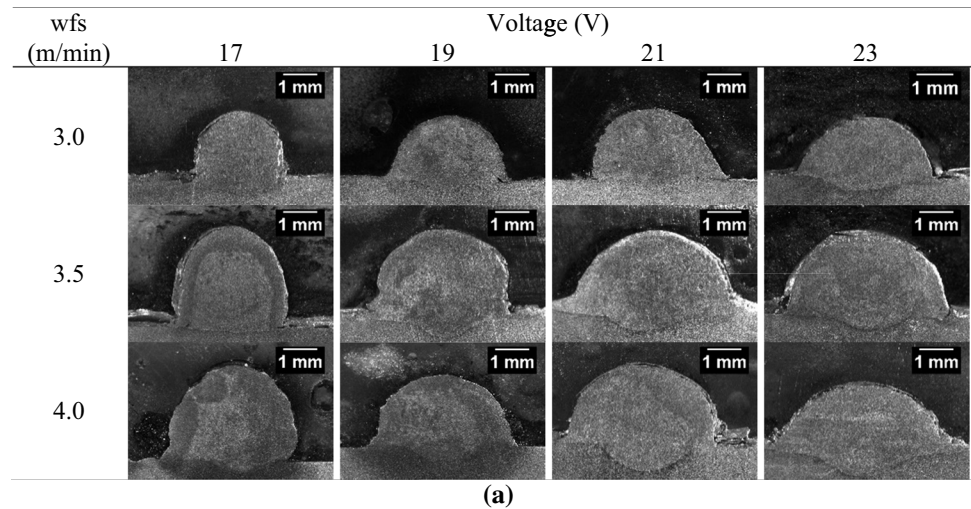
For analysing the microstructure, samples were taken from the mid regions of the deposited wall. The standard metallography procedure was followed to prepare the samples. The microstructural analysis was performed using an optical microscope (Leica, DM ILM), and the grain sizes were measured using ImageJ software. The microstructure of the deposited wall followed the typical pattern of a multilayer weld deposition. In general, the Widmanstätten structure forms in the single-pass bead welding [29]. In the AM process, the deposited wall undergoes through multiple heating and cooling cycles due to layer by layer deposition. Therefore, only the top region retains the Widmanstätten structure, and the remaining region gains the normalised weld structure. Baufeld et al. [30] also observed coarsening of grains due to repeated heating, except for the top region.

Table 4 shows the observed microstructure of the deposited wall for three different regions, i.e. bottom, middle and top. The grain size was approximately from 2 to 9 μm , below 5 μm is referred here as finer and above as coarser. The microstructure in the middle and top regions appeared similar in all the cases, i.e. grains were coarse in the middle regions (6.95–8.7 μm) and relatively finer in top regions (2.03–4.25 μm). In the bottom regions, the grains were formed coarse in case of substrate-1 and 2 (7.4 and 6.41 μm). However, in the case of substrate-3 and 4, the microstructure was found finer (5.25 and 2.03 μm) as compared to the other two substrates. These microstructural variation could be the result of the difference in cooling rate associated with the individual substrates. In general, the microstructure associated with high cooling rate yields finer grains as compared with low cooling rate [31]. The finer microstructure found in the case of bottom layers of substrate-3 and 4 could be the outcome of high cooling rate due to bulk mass at the substrate.

3.4 Micro Indentation Hardness Study

The micro indentation hardness (Vickers hardness, model: UHL VMHT) study was performed across the height of the deposited wall. The applied load was 100 gf for a duration of 15 s. The top regions of the deposited wall showed relatively more hardness as compared to the middle and bottom

Fig. 4 a cross-section images of beads deposited at different voltage and wire feed speed, b Variation of the bead width and height with the input voltage for different wire feed rates



regions. The similar trend was observed for both pillar-based substrate and the solid substrate. The hardness of the deposited walls was found to be varying in the range of 180–240 HV (Fig. 6). This variation in hardness could be because of the change in the microstructure discussed in the preceding section. In general, the finer grains yield relatively more hardness as compared to coarser grains, e.g. the top regions had finer grains imparting more hardness than the bottom and middle regions, which had a coarser grain (Table 4). Substrate-1 was not considered for this study for its similarity with substrate-2.

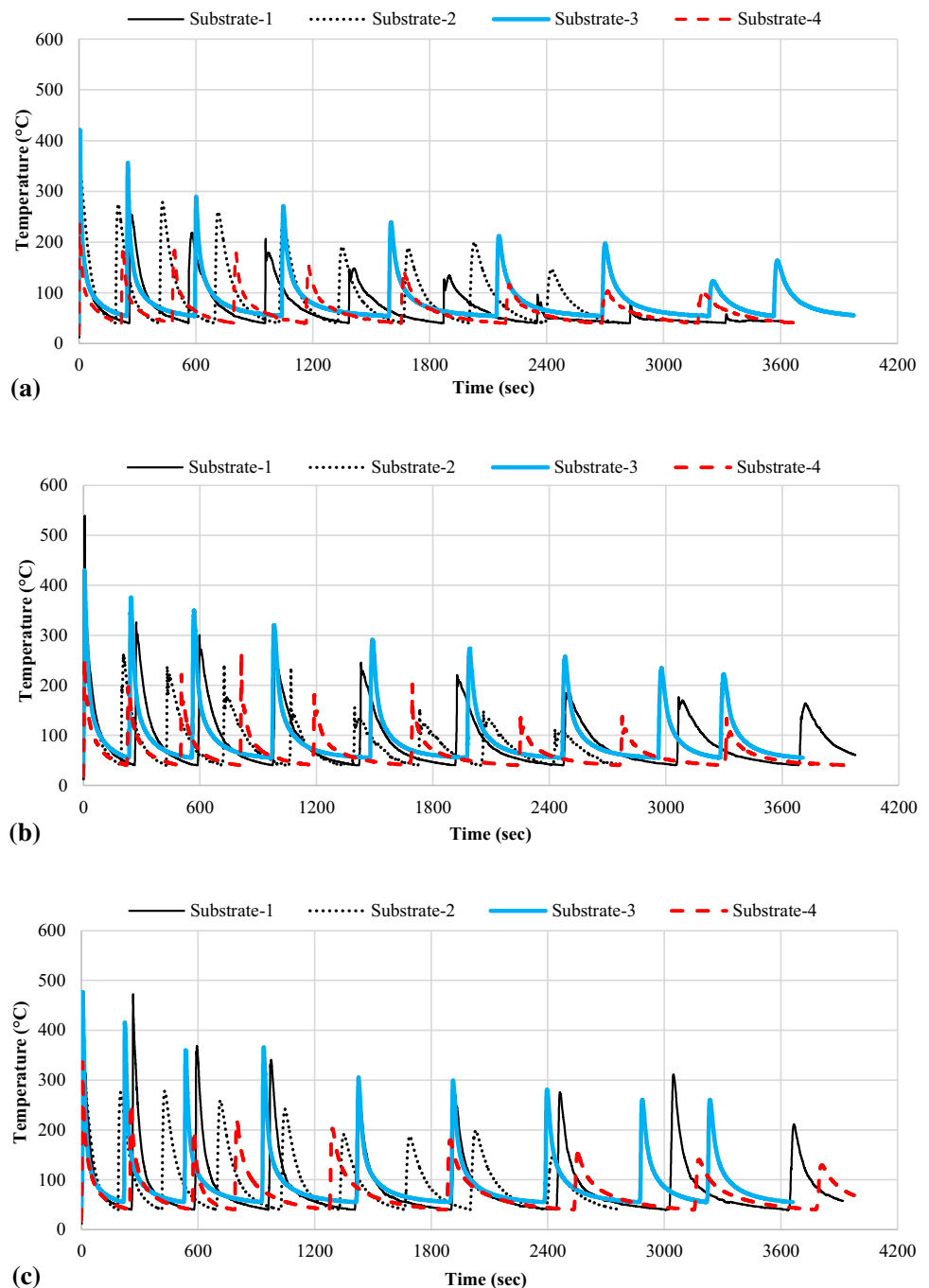
3.5 Effectiveness of Pillar-Based Substrate in Part Removal and Reducing Material Wastage

The experiments were further extended for the fabrication of two-dimensional structures on the substrate-5 (Fig. 7). Figure 7a shows the substrate assembly by two-dimensional fastening through nut and bolts in two perpendicular holes made in the pillars. The mechanical fastening ensures that the assembled pillar-based substrate would act similar to

the solid substrate during the deposition. The actual substrate used is shown in Fig. 7b. Figure 7c shows the two parts selected for the deposition, i.e. a hollow cylinder of diameter 100 mm and a square part of side 50 mm. Here the cylinder was deposited first and then the square part inside it. However, alternate methods could also be used, such as depositing both the parts simultaneously, layer by layer, and depositing the square part first and then the cylinder. The appropriate method could be chosen depending upon part geometry, ensuring the deposition head must reach in the selected regions.

Since the parts were hollow, they could be deposited on the same substrate. Both parts were deposited using the optimised parameters. Negligible deformation in the substrate was observed. After deposition, both the parts were easily disassembled from the substrate. As the substrate was temporarily assembled, it was separated without any machining. The deposited part obtained had pillar substrates attached only at the part boundary (Fig. 7d and e). In this case, the removal and finishing were much easier as compared to a part deposited on a conventional substrate. Deposition of


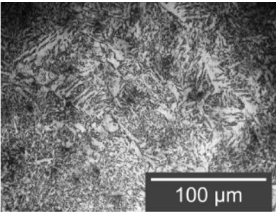
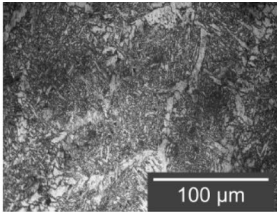
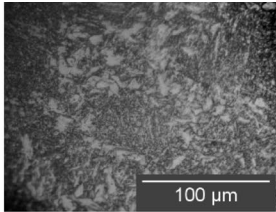
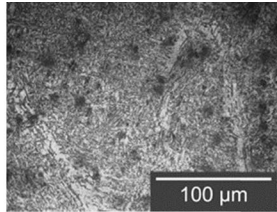

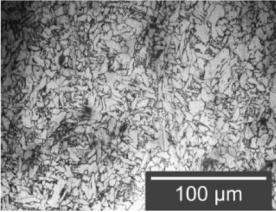
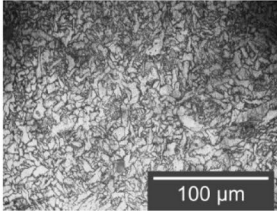
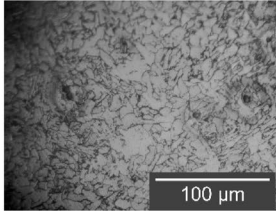
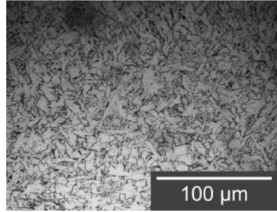

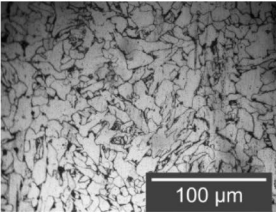
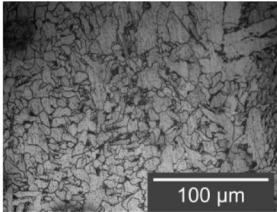
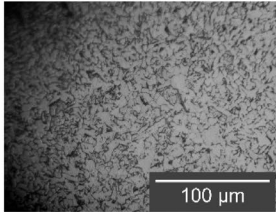
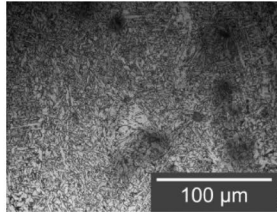
Fig. 5 Temperature pattern during wall deposition for Substrate-1 to Substrate-4 at **a** a distance of 5 mm from the start point, **b** the middle, and **c** a distance of 5 mm before endpoint

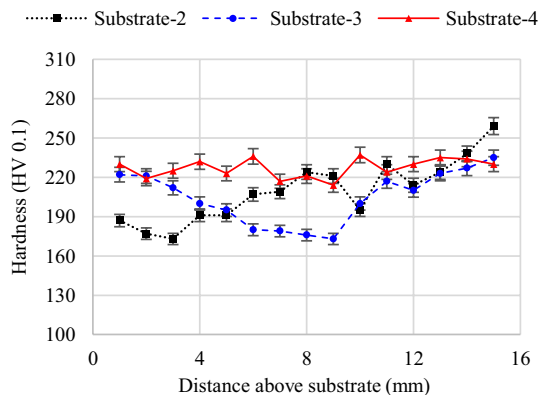


two parts, one inside another, and their easy separation shows the effectiveness of pillar-based substrate in utilising the deposition area more adequately. The pillar substrates left unused or not representing the cross-section of the base of the part fabricated were available for reuse (Fig. 7f). Similar combinations of multiple cuboidal pillars could be made to form the desired deposition surface.

Cost comparison for part separation and finishing was carried between the pillar-based and solid substrate. The pillar-based substrate was found to be approximately 75% effective in terms of cost when compared with solid substrate. It was calculated in terms of direct labour, material and energy for part separation and finishing. The part separation was found to be differentiating the two process significantly, whereas finishing requirement would remain the same.

Table 4 Comparison of the microstructure of the deposited wall on different substrates in various regions

Location on cross-section	Substrate-1	Substrate-2	Substrate-3	Substrate-4
				
				
				

**Fig. 6** Measured micro indentation hardness above the substrate of the deposited wall

3.6 The Pillar-Based Substrate to Support Overhanging Features

Support structures are often required to deposit an overhanging feature. The pillar-based substrates could also be utilised to support the overhanging portion of the part by employing pillars of different geometrical aspects depending on the part geometry. In this study, a simple ‘V’ shaped structure with a slope of 20° was chosen for the demonstration. It could be achieved by using the cuboidal pillars of varying heights, as shown in Fig. 2g (substrate-6). Here, the chosen

cross-section of the pillars was 8 × 8 mm, with the height varying from 15 to 33 mm in steps of 3 mm. Deposition on this up and down slopes shows the capability of the pillar-based substrate to make overhanging features. The pillars reduced the requirement of any additional support structures as the substrate could act as the needed support. This approach may not be limited to axis-symmetric parts and requires only 3-axis motion to deposit complex geometries. Similarly, the cross-section area of the pillar and step height could be varied to achieve the desired bead dimensions and overhanging feature.

During the deposition, it was observed that the downward slope showed uniform deposition, and the upward slope showed relatively non-uniform deposition (Fig. 8a). The difference in downward and upward slope deposition could be because of the fluidity behaviour of the molten metal under the arc pressure and the acting gravitational force. In the case of the downward slope deposition, these forces carried the molten metal backward against gravity. Whereas in the case of upward slope deposition, it acts to bring the molten metal further downward. This particular behaviour of the deposition was initiated from the initial layer, which was further propagated. From Fig. 8a, it could be seen that the molten metal was reaching in the pillar step corners for downward slope, resulting in a uniform deposition. However, the step corners were almost left from receiving any material in case of the upward slope. It resulted in a non-uniform deposition for the upward slope. However, it can be nullified

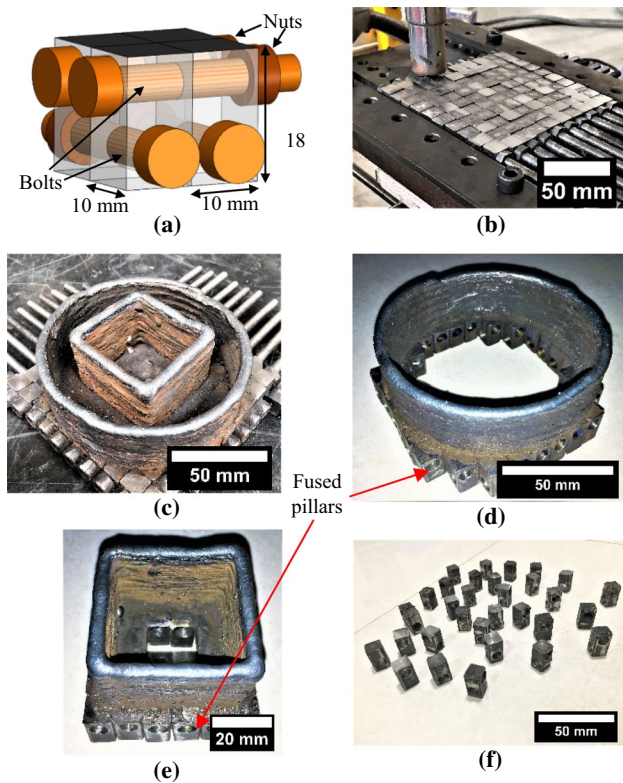


Fig. 7 **a** CAD model representing the pillar-based substrate assembly consisting of four pillars, and pictorial view of **b** pillar-based substrate fastened to form a square surface, **c** hollow square and cylindrical parts deposited on the substrate, **d** and **e** disassembled parts, **f** remaining pillars available for reuse after the part separation

by following the deposition strategy of changing the start point of deposition in alternate layers. The deposited part is shown in Fig. 8b. Figure 8c shows the height of each layer after deposition and verifies the same height at the start and endpoint. The step height for overhanging deposition may need to be optimised depending on geometrical features. In order to enhance the dimensional accuracy, lesser step height, and step size (cross-section area of a pillar) could be used. Based on this experimental investigation, it could be proposed that the approach would be equally applicable for other AM processes irrespective of utilised material form (powder or wire) and fusion sources such as the laser, electron beam and arc.

4 Conclusion

An approach called pillar-based substrate has been successfully demonstrated to facilitate easy part removal in WAAM. The cuboidal pillar (substrate-3) performed better among the different design approaches when compared with the conventional substrate. It was confirmed by analysing the

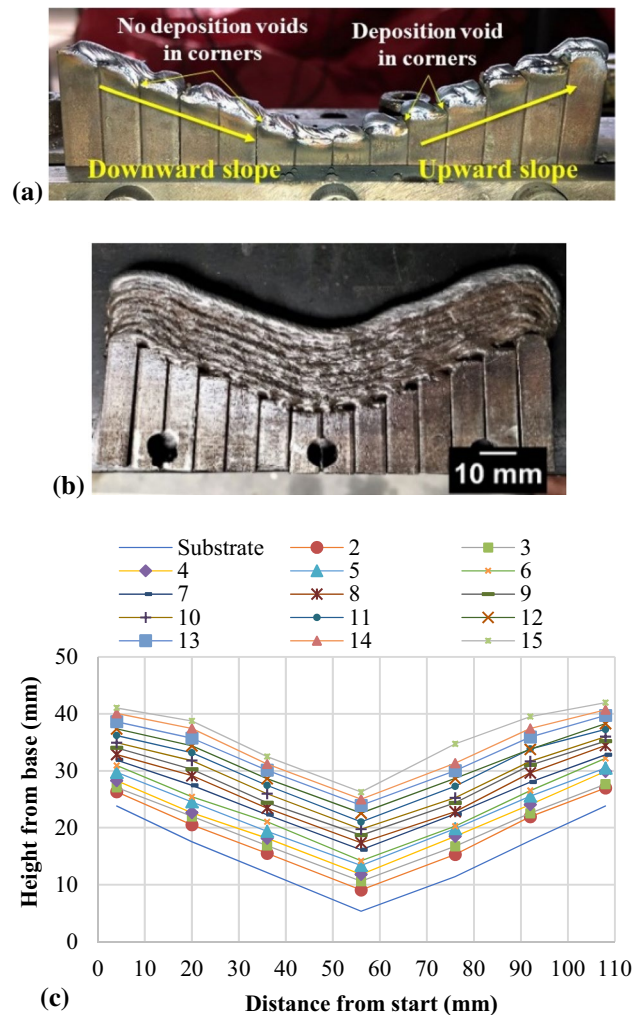


Fig. 8 Pictorial view of **a** the deposited first layer, **b** the deposited part (with alternative start and endpoint), and **c** measured the height of each deposited layer (2–15) along with the substrate at different locations

temperature profiles measured at the substrate, the microstructural study and the hardness test. In the pillar-based substrate, the cooling time was found to be in similar ranges while the peak temperatures were relatively higher than the solid substrate. It shows the proposed substrate is equally capable of dissipating the generated heat. The microstructural study revealed that the grain structure patterns were consistent, i.e. finer at the top regions, coarser at the bottom and middle regions. The measured micro indentation hardness was found to be in the range of 180–240 HV, where the top region always yielded relatively higher hardness for all the cases. Since the properties of the parts deposited on the pillar-based substrate were analogous with that on the conventional substrate, it was assured that pillar-based substrate could be reliably used with little effects on part quality. Further, the pillar-based substrates were arranged in an array

to form the larger surface area. The deposition of a hollow cylinder and a square part was demonstrated on the same substrate and disassembled without any machining. The pillars that were remained intact from receiving any deposition or not representing the cross-section of the base of the deposited part can be reused. The deposition of overhanging features was also successfully demonstrated by varying the pillar heights. The approach showed good potential to facilitate ease of part removal, minimise material wastage and act as an effective support mechanism.

Acknowledgement The authors would like to thank the technical staff of the Central Workshop and the Department of Mechanical Engineering, IIT Indore, for their extended help and support. They also thank Dr Satyajit Chatterjee for allowing to access the Tribology Laboratory facilities.

Funding This research did not receive any specific grant from funding agencies in the public, commercial, or not-for-profit sectors.

References

- Lee, C. M., Woo, W. S., Baek, J. T., & Kim, E. J. (2016). Laser and arc manufacturing processes: A review. *International Journal of Precision Engineering and Manufacturing*, 17(7), 973–985. <https://doi.org/10.1007/s12541-016-0119-4>
- Jinoop, A. N., Subbu, S. K., Paul, C. P., & Palani, I. A. (2019). Post-processing of laser additive manufactured inconel 718 using laser shock peening. *International Journal of Precision Engineering and Manufacturing*, 20(9), 1621–1628. <https://doi.org/10.1007/s12541-019-00147-4>
- Kim, J., Lee, W. J., & Park, H. W. (2016). The state of the art in the electron beam manufacturing processes. *International Journal of Precision Engineering and Manufacturing*, 17(11), 1575–1585. <https://doi.org/10.1007/s12541-016-0184-8>
- Ha, S., Park, E., & Kim, N. (2020). Analysis of shape deformation from densification of additive manufacturing parts in selective laser sintering. *International Journal of Precision Engineering and Manufacturing*, 21(8), 1571–1580. <https://doi.org/10.1007/s12541-020-00359-z>
- Lee, C. M., Woo, W. S., Kim, D. H., Oh, W. J., & Oh, N. S. (2016). Laser-assisted hybrid processes: A review. *International Journal of Precision Engineering and Manufacturing*, 17(2), 257–267. <https://doi.org/10.1007/s12541-016-0034-8>
- Ding, D., Pan, Z., Cuiuri, D., & Li, H. (2015). Wire-feed additive manufacturing of metal components: Technologies, developments and future interests. *International Journal of Advanced Manufacturing Technology*, 81(1–4), 465–481. <https://doi.org/10.1007/s00170-015-7077-3>
- Wang, Z., Jing, T., & Dong, H. (2019). Phase field study of spacing evolution during wire and laser additive manufacturing under transient conditions. *IOP Conference Series Materials Science and Engineering*. <https://doi.org/10.1088/1757-899X/529/1/012003>
- Nie, Z., Wang, G., McGuffin-Cawley, J. D., Narayanan, B., Zhang, S., Schwam, D., & Rong, Y. (2016). Experimental study and modeling of H13 steel deposition using laser hot-wire additive manufacturing. *Journal of Materials Processing Technology*, 235, 171–186. <https://doi.org/10.1016/j.jmatprotec.2016.04.006>
- Wu, B., Pan, Z., Ding, D., Cuiuri, D., Li, H., Xu, J., & Norrish, J. (2018). A review of the wire arc additive manufacturing of metals: Properties, defects and quality improvement. *Journal of Manufacturing Processes*, 35, 127–139. <https://doi.org/10.1016/j.jmapro.2018.08.001>
- Montevecchi, F., Venturini, G., Grossi, N., Scippa, A., & Campatelli, G. (2018). Idle time selection for wire-arc additive manufacturing: A finite element-based technique. *Additive Manufacturing*, 21, 479–486. <https://doi.org/10.1016/j.addma.2018.01.007>
- Xiong, J., Lei, Y., Chen, H., & Zhang, G. (2017). Fabrication of inclined thin-walled parts in multi-layer single-pass GMAW-based additive manufacturing with flat position deposition. *Journal of Materials Processing Technology*, 240, 397–403. <https://doi.org/10.1016/j.jmatprotec.2016.10.019>
- Panchagnula, J. S., & Simhambhatla, S. (2018). Manufacture of complex thin-walled metallic objects using weld-deposition based additive manufacturing. *Robotics and Computer-Integrated Manufacturing*, 49, 194–203. <https://doi.org/10.1016/j.rcim.2017.06.003>
- Ding, D., Pan, Z., Cuiuri, D., & Li, H. (2014). A tool-path generation strategy for wire and arc additive manufacturing. *International Journal of Advanced Manufacturing Technology*, 73(1–4), 173–183. <https://doi.org/10.1007/s00170-014-5808-5>
- Abe, T., & Sasahara, H. (2015). Development of the shell structures fabrication CAM system for direct metal lamination using arc discharge-lamination height error compensation by torch feed speed control-. *International Journal of Precision Engineering and Manufacturing*, 16(1), 171–176. <https://doi.org/10.1007/s12541-015-0022-4>
- Wu, B., Ding, D., Pan, Z., Cuiuri, D., Li, H., Han, J., & Fei, Z. (2017). Effects of heat accumulation on the arc characteristics and metal transfer behavior in wire arc additive manufacturing of Ti6Al4V. *Journal of Materials Processing Technology*, 250, 304–312. <https://doi.org/10.1016/j.jmatprotec.2017.07.037>
- Geng, H., Li, J., Xiong, J., Lin, X., & Zhang, F. (2017). Optimization of wire feed for GTAW based additive manufacturing. *Journal of Materials Processing Technology*, 243, 40–47. <https://doi.org/10.1016/j.jmatprotec.2016.11.027>
- Martina, F., Colegrove, P. A., Williams, S. W., & Meyer, J. (2015). Microstructure of interpass rolled wire + arc additive manufacturing Ti-6Al-4V components. *Metallurgical and Materials Transactions A: Physical Metallurgy and Materials Science*, 46(12), 6103–6118. <https://doi.org/10.1007/s11661-015-3172-1>
- Martina, F., Mehnen, J., Williams, S. W. W., Colegrove, P., & Wang, F. (2012). Investigation of the benefits of plasma deposition for the additive layer manufacture of Ti-6Al-4V. *Journal of Materials Processing Technology*, 212(6), 1377–1386. <https://doi.org/10.1016/j.jmatprotec.2012.02.002>
- Venturini, G., Montevecchi, F., Scippa, A., & Campatelli, G. (2016). Optimization of WAAM deposition patterns for T-crossing features. *Procedia CIRP*, 55, 95–100. <https://doi.org/10.1016/j.procir.2016.08.043>
- Azizi, A., & Schiffres, S. N. (2020). Laser metal additive manufacturing on graphite. *Solid Freeform Fabrication 2018: Proceedings of the 29th Annual International Solid Freeform Fabrication Symposium - An Additive Manufacturing Conference, SFF 2018*, 2315–2324.
- Hildreth, O. J., Nassar, A. R., Chasse, K. R., & Simpson, T. W. (2016). Dissolvable metal supports for 3D direct metal printing. *3d Printing and Additive Manufacturing*, 3(2), 91–97. <https://doi.org/10.1089/3dp.2016.0013>
- Haselhuhn, A. S., Wijnen, B., Anzalone, G. C., Sanders, P. G., & Pearce, J. M. (2015). In situ formation of substrate release mechanisms for gas metal arc weld metal 3-D printing. *Journal of Materials Processing Technology*, 226, 50–59. <https://doi.org/10.1016/j.jmatprotec.2015.06.038>
- Haselhuhn, A. S., Gooding, E. J., Glover, A. G., Anzalone, G. C., Wijnen, B., Sanders, P. G., & Pearce, J. M. (2016). Substrate

- release mechanisms for gas metal arc weld 3D aluminum metal printing. *3D Printing and Additive Manufacturing*, 1(4), 204–209. <https://doi.org/10.1089/3dp.2014.0015>
24. Jiang, J., Xu, X., & Stringer, J. (2018). Support structures for additive manufacturing: A review. *Journal of Manufacturing and Materials Processing*, 2(4), 64. <https://doi.org/10.3390/jmmp2040064>
 25. Kapil, S., Joshi, P., Kulkarni, P. M., Negi, S., Kumar, R., & Karunakaran, K. P. (2018). Elimination of support mechanism in additive manufacturing through substrate tilting. *Rapid Prototyping Journal*, 24(7), 1155–1165. <https://doi.org/10.1108/RPJ-07-2017-0139>
 26. Kazanas, P., Deherkar, P., Almeida, P., Lockett, H., & Williams, S. (2012). Fabrication of geometrical features using wire and arc additive manufacture. *Proceedings of the Institution of Mechanical Engineers, Part B: Journal of Engineering Manufacture*, 226(6), 1042–1051. <https://doi.org/10.1177/0954405412437126>
 27. Xia, C., Pan, Z., Polden, J., Li, H., Xu, Y., & Chen, S. (2021). Modelling and prediction of surface roughness in wire arc additive manufacturing using machine learning. *Journal of Intelligent Manufacturing*. <https://doi.org/10.1007/s10845-020-01725-4>
 28. Cunningham, C. R., Flynn, J. M., Shokrani, A., Dhokia, V., & Newman, S. T. (2018). Invited review article: Strategies and processes for high quality wire arc additive manufacturing. *Additive Manufacturing*, 22(June), 672–686. <https://doi.org/10.1016/j.addma.2018.06.020>
 29. Weman, K. (2012). *Welding processes handbook*. (2nd ed.). Woodhead Pub.
 30. Baufeld, B., Van der Biest, O., & Gault, R. (2010). Additive manufacturing of Ti–6Al–4V components by shaped metal deposition: Microstructure and mechanical properties. *Materials & Design*, 31, S106–S111. <https://doi.org/10.1016/J.MATDES.2009.11.032>
 31. Keehan, E., Zachrisson, J., & Karlsson, L. (2010). Influence of cooling rate on microstructure and properties of high strength steel weld metal. *Science and Technology of Welding and Joining*, 15(3), 233–238. <https://doi.org/10.1179/136217110X12665048207692>

Publisher's Note Springer Nature remains neutral with regard to jurisdictional claims in published maps and institutional affiliations.



Anas Ullah Khan is a Ph.D. scholar in the Department of Mechanical Engineering of IIT Indore, India. He is working in the area of wire arc additive manufacturing. He obtained an M.E. degree in CAD/CAM/CAE in 2018 from SGSITS Indore, India and B.Tech degree in Mechanical Engineering from JUET Guna, India, in 2016. He has co-authored several papers in the area of wire arc additive manufacturing and its control.



Yuvraj K Madhukar is an Assistant Professor in the Department of Mechanical Engineering, IIT Indore. He received his Ph.D. from IIT Kharagpur in 2016. He was a Research Associate during 2015–2017 in Heriot-Watt University, Edinburg, U.K. His area of research includes water-assisted laser material processing, wire arc additive manufacturing and its control. He has co-authored several journal and conference papers and a book chapter.